

# 3 D Nonlinear Finite Element/Fracture Mechanics Analysis of Pressurized Nuclear Reactor Container Ring

Victor E. Saouma<sup>a,\*</sup> Eric Hansen<sup>a</sup>,

<sup>a</sup>*Dept. of Civil Engineering, University of Colorado, Boulder*

---

## Abstract

Nuclear reactor containers, without inner liners, must withstand internal pressurization with minimal leak to the outside through the cracks. This paper reports on a 3D finite element simulation of a prestressed nuclear reactor container ring subjected to internal pressure. Discrete cracks are used, and the effect of crack surface pressurization on crack openings is investigated.

It is shown that the discrete crack model can provide a suitable alternative to the smeared crack one, and that for the selected ring, the effect of additional crack pressurization is minimal.

*Key words:* Nuclear Reactor; Finite Element; Fracture Mechanics.

---

## 1 Introduction

Nuclear reactor container vessels, without internal steel lining, must undergo, (approximately every 10 years) a test to assess the extent (if any) of internal cracking which may result in gas leak to the outside. However, there is concern that the repetition of these pressure tests may accelerate internal cracking since the maximum applied pressure is well above the normal operating one.

Given the potential for test induced cracks, it is desirable to perform a realistic finite element (FE) simulation of the container pressurization. Not only is it important that the FE model properly simulates the internal cracking, but it is of paramount importance

---

\* Corresponding Author.

(especially if cracking initiates from the interior) that the model can simulate the application of the internal pressure on the faces of the propagating crack. If this additional crack driving traction is ignored, then an unconservative analysis may result.

With regard to nonlinear finite element modeling of nuclear reactors, there was indeed a tremendous amount of related activities in the 60's, till the 80's. At the time, most of the emphasis was on modeling the compressive response of concrete based on plasticity models. Tensile response was, for the most part, handled by the smeared crack model first proposed by Rashid (1968) specifically for the analysis of containers. Most recently, there appear to have been on the one hand a decline in general interest in FE modeling of nuclear reactors, and on the other hand an explosion in research related to modeling concrete cracking.

Ever since the pioneering work of Bažant, Z.P. and Cedolin, L. (1979), there has been a recognition that: 1) unobjective results will be obtained if tensile stresses are merely limited to the tensile strength without adjustment for mesh size; and 2) concrete fails as a quasibrittle material, (Hillerborg, A. and Modéer, M. and Petersson, P.E. 1976). This in turn, has sparked much interest in the research community. The main challenge confronting the computational community has been how to localize a (smeared) crack in an objective manner, and if possible derive a “unified” constitutive model for tension and compression. This line of research has been most often presented at the FramCoS (Fracture Mechanics of Concrete Structures) conferences, (deBorst, Mazars, Pijaudier-Cabot and vanMier 2001). Some of the most recent and popular techniques include: Damage Mechanics (where the emphasis is on stiffness degradation rather than strength) (Mazars 1984); Microplane model, where the constitutive law is expressed in terms of stress and strain vectors rather than tensors, (Carol, Prat and Lopez 1997); Nonlocal continuum where the stress at a point depends on the strain history within a non-zero interaction radius; or combinations of the above (Hansen, Willam and Carol 2001). Most of these papers stem from a continuum mechanics/plasticity approach.

Invariably, most of the preceding papers begin with a statement indicating that whereas a discrete crack may be a more suitable model, its implementation (in the context of a non-linear analysis) would be too cumbersome to develop in light of the need to continuously remesh. As a result, some of the most innovative recent research have focused on alternate methods to model explicitly a discrete crack without remeshing, (Oliver, Huespe, Pulido and Chaves 2002), (Belytschko, T. and Moës and Usui, S. and Parimi, C. 2001), (Jirasek and Bažant 2001). These models are undoubtedly extremely powerful and promising, yet to the best of the author's knowledge, none of them has yet been reported in a context other than a simplified linear elastic test problem. Their capability to handle “real-world” practical problems in the context of a full 3D, non-linear analysis (including multiple cracks, non-linear continuum, crack pressurization) remains to be proven.

Which brings us back to the discrete crack model. It is well known that this was the first one adopted in the pioneering work of (Sims, Rhodes and Clough 1964) and (Ngo and Scordelis 1967), but which was later dethroned by the smeared crack model of Rashid

(1968), and the simplicity of its implementation as we were rapidly moving from the earlier linear elastic analysis to nonlinear ones, (Nilson 1968). The discrete crack model was revived by (Saouma 1980), but its use has remained confined to the work at Cornell (where 3D problems appear to be addressed through a combination of linear finite and boundary elements) and the University of Colorado.

The discrete crack model implement by our group hinges on the finite element analysis program MERLIN (Reich, Červenka and Saouma 1997) at the kernel and is surrounded by other codes for mesh generation, crack propagation monitoring, and visualization of results.

Merlin is a 3D static/dynamic finite element code supporting well over 20 different element types, 12 constitutive models, and various nonlinear algorithms. Originally developed for the fracture analysis of dams, it has recently been extended to include reinforced concrete. It supports both discrete cracks, (Cervenka, Chandra Kishen and Saouma 1998) and smeared cracks (Hansen and Saouma 2002), and one of its major features is its ability to apply pressure on that portion of the crack which is opened (originally developed to simulate uplift pressures in dams).

Hence, the objective of this paper is to use a discrete crack model to simulate the pressurization (and failure) of a prestressed nuclear reactor container ring with crack pressurization.

## 2 Problem Description

The problem selected is a fictitious (but realistic) ring which does not correspond to any nuclear reactor vessel. The ring has an internal radius of 22,500 mm, and an external one of 23,400 mm. The prestressing tendon is at a radius of 23,150 mm. There are two opposite ribs which house the tendon anchors. The concrete has an elastic modulus  $E$  of 31,000 MPa, Poisson's ratio of 0.22, mass density of 2,500 Kg/m<sup>3</sup>, compressive strength  $f'_c$  of 38.3 MPa, and a tensile strength of 4 MPa. The steel reinforcement consists of four 25 mm diameter rebars with an elastic modulus of 190,000 MPa, Poisson's ratio of 0.3, mass density of 7,850 Kg/m<sup>3</sup>, and a yield stress  $f_y$  equal to 500 MPa. The prestressing steel consists of two tendons,  $A_{ps}$  equal to 5,143 mm<sup>2</sup> each, initial prestressing force of 4.4 MN, elastic modulus of 190,000 MPa, Poisson's ratio of 0.3, mass density of 7,850 Kg/m<sup>3</sup>, and a yield stress  $f_y$  equal to 1,814 MPa. Finally, the vertical prestressing is 8.5 MPa.

The ring cross section (away from the anchor zones) is shown in Fig. 1.

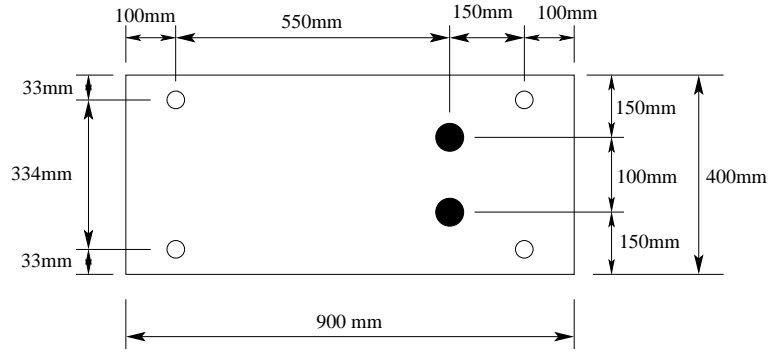


Fig. 1. Cross Section of Container Ring

### 3 Discretization

#### 3.1 Assumptions

For this problem, the following simplifying assumptions are made:

- (1) Perfect bond between steel and concrete (bond slip could indirectly be accounted for by reducing the steel elastic modulus), and reinforcement is composed of 3D truss elements.
- (2) Initial prestressing is accounted for by specifying a coefficient of thermal expansion  $\alpha$  equal to unity for the prestressing steel, and a temperature drop equal to the prestressing force divided by the steel's Young modulus.
- (3) In all analyses, the first load increment applies the prestressing force (through nodal equivalent temperature), and vertical prestressing as surface traction.
- (4) In all subsequent increments, internal pressurization is gradually increased. The vertical tractions are reduced in relation to the increase in internal pressure to simulate the effect of the closed container cap (see Appendix ??).
- (5) Correctness of load application and boundary conditions is (partially) confirmed through the graphical displays of the deformed mesh (symmetric).

#### 3.2 Meshes

The FE mesh was created using the mesh generator Kumonosu, (Hansen and Saouma 2001) developed by our group. Kumonosu has the capability to define FE mesh boundaries using true curves, thus allowing the model to be defined by the ring's actual geometry. The 3D boundary description for the ring model is shown in Fig. 2.

The resulting FE mesh, consisting of 6,046 nodes, 2,564 1D truss elements to model the passive and active steel, and 23,370 3D tetrahedral elements to model the concrete continuum, is shown in Fig. 3.

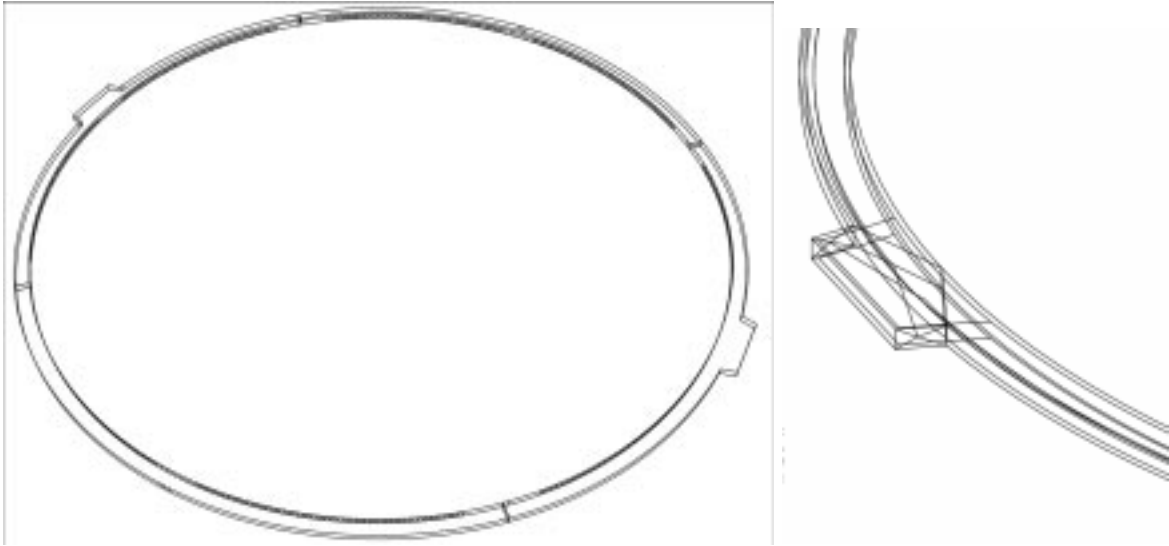


Fig. 2. Boundary Description for 3D Ring Mesh

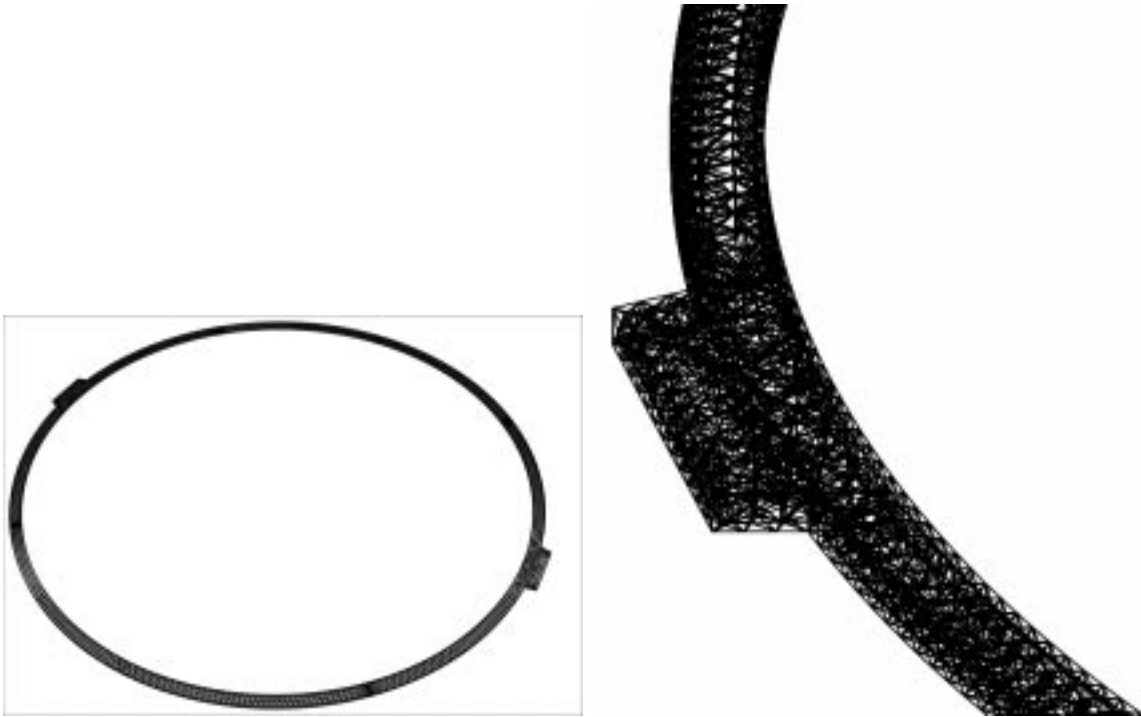


Fig. 3. FE Mesh for 3D Ring Model

### 3.3 *Material parameters*

Material parameters for the concrete continuum, passive reinforcement, prestressing steel, and discrete cracks for the nonlinear analyses are summarized in Table 3.3.

Property	Symbol	Value	Units
Concrete continuum - Linear elastic			
Elastic modulus	$E$	3.100e+004	MPa
Poisson ratio	$\nu$	0.22	
Coeff. of thermal expansion	$\alpha$	0.0	$/^{\circ}C$
Passive reinforcement - $J_2$ plasticity			
Elastic modulus	$E$	1.900e+005	MPa
Poisson ratio	$\nu$	0.0	
Coeff. of thermal expansion	$\alpha$	0.0	$/^{\circ}C$
Yield stress	$\sigma_y$	500.0	MPa
Hardening modulus	$H$	0.0	
Prestressing steel - Linear elastic			
Elastic modulus	$E$	1.900e+005	MPa
Poisson ratio	$\nu$	0.0	
Coeff. of thermal expansion	$\alpha$	4.503e-005	$/^{\circ}C$
Discrete cracks - Interface Crack Model			
Tangential stiffness	$K_T$	3.100e+005	MPa/m
Normal stiffness	$K_N$	3.100e+005	MPa/m
Tensile strength	$f'_t$	4.0	MPa
Cohesion	$c$	5.0	MPa
Angle of friction	$\phi_f$	45.0	degrees
Dilatancy angle	$\phi_d$	20.0	degrees
Mode I fracture energy	$G_F^I$	100.0	N/m
Mode II fracture energy	$G_f^{IIa}$	1000.0	N/m
Break point stress for bilinear softening	$s_1$	1.0	MPa
Break point COD for bilinear softening	$sw_1$	1.875e-005	m
Break point cohesion for bilinear softening	$c_1$	1.25	MPa
Break point CSD for bilinear softening	$cw_1$	1.5e-004	m

Table 1  
Material Parameters for Nonlinear Ring Analysis

## 4 Analysis procedure

Analysis of the ring begins with the application of the prestressing, both radial and vertical. The vertical prestressing is simply applied as a traction to the upper surfaces of the ring. The radial prestressing is applied by changing the temperature of those elements which comprise the prestressing cables. Each prestressing cable has an initial tension of 4.4 MN. Given the cable elastic modulus of  $19.0 \times 10^4$  MPa and cross sectional area of  $5,143 \text{ mm}^2$ , this initial tension is equal to an initial strain of  $1.191 \times 10^{-7}$ . Since thermal strains are equal to  $\epsilon = \alpha \Delta T$ , the coefficient of expansion  $\alpha$  can be determined for a given change in temperature. The temperature change was assumed to be  $\Delta T = -100^\circ\text{C}$  (negative in order to apply a compressive force to the ring), which results in a coefficient of expansion of  $\alpha = 4.5028 \times 10^{-5}/^\circ\text{C}$  for the prestressing cables.

The displacement boundary conditions for each ring analysis are summarized in Fig. 4.

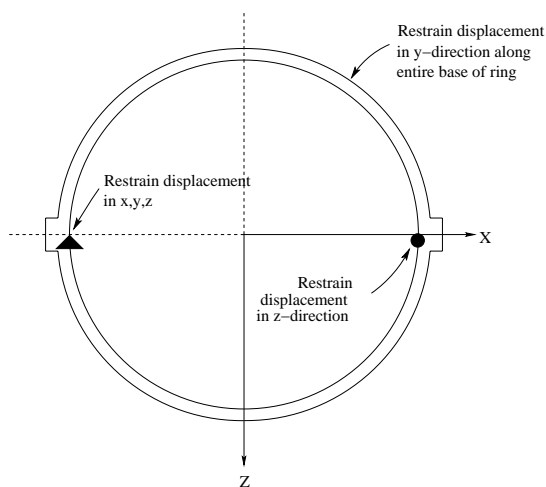


Fig. 4. Ring analysis fixed boundary conditions

The analysis procedure for all cases is as follows:

- (1) Prescribe a vertical compressive traction of 8.5 MPa to the upper surface of the ring and prescribe a temperature change of  $\Delta T = -100^\circ\text{C}$  to the prestressing steel elements.
- (2) For the subsequent increments,
  - (a) Prescribe a traction normal to the interior surfaces of the ring equal to  $\Delta p = 0.1$  MPa. Additionally, prescribe a vertical tensile traction of  $\Delta p = 0.613$  MPa to the upper surface of the ring to simulate the cap effect.
  - (b) For the analysis which includes the effect of pressurization of the discrete cracks, internal pressures are applied to the cracks such that the internal pressure is equal to the internal ring pressure,  $\Delta p = 0.1$  MPa. Uplift pressures are defined as  $p = \gamma h$ , where  $\gamma$  is the fluid weight per volume and  $h$  is the fluid height. In this case,  $\gamma = 0.001$  and  $h = 1000x\Delta p$ . Such a large “height” is needed in this

case to insure that the internal pressure is constant throughout the height of the ring.

## 5 Analyses

Three analyses were performed to evaluate the performance of the ring:

- (1) A linear elastic analysis with an uncracked mesh to determine the internal pressure required to initiate cracking and the locations of the crack nucleations.
- (2) A nonlinear analysis with a cracked mesh to determine the internal pressure required to provide sufficient crack opening for gasses to escape from the container.
- (3) A second nonlinear analysis with a cracked mesh which considers the effects of pressurization on the faces of the cracks.

### 5.1 Linear elastic analysis to locate cracking

This first analysis seeks to determine the locations of crack initiation and the internal pressure at which the cracks initiate. To accomplish this, the ring materials are assumed to be linear elastic, the prestressing force is first applied, and then the internal pressure in the ring is increased until the circumferential principal stress  $\sigma_{\theta\theta}$  at the ring interior exceeds the tensile strength of the concrete,  $f'_t = 4$  MPa.

Examination of the principal stresses indicates that cracking is most likely to occur in the four sectors marked by the arrows in Fig. 5. The MERLIN analysis results show that the

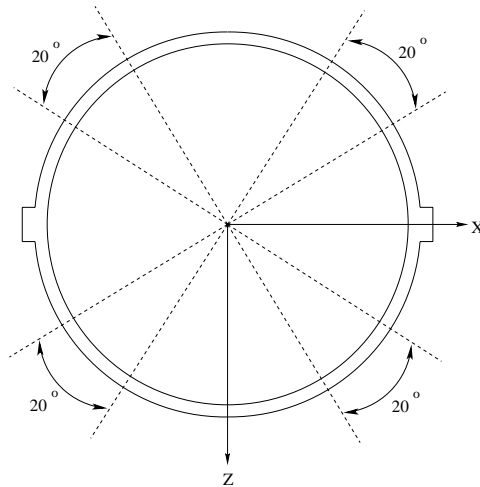


Fig. 5. Sectors of probable crack initiation

$\sigma_{\theta\theta}$  stress in the sectors indicated in Fig. 5 are 4.5 MPa on average at an internal pressure of 1.2 MPa. This agrees quite well with the stress estimate determined in Appendix ??

by the thick-walled cylinder equations. Thus, we conclude that crack initiation will occur at angles of  $\pi/4$  (center of each sector in Fig. 5) relative to the ring center at an internal pressure  $p = 1.2$  MPa.

## 5.2 *Nonlinear analyses with and without crack pressurization*

The next two analyses consider the response of the cracked mesh subject to the loading procedure outlines in Appendix 4. While the concrete continuum and prestressing steel are assumed to be linear elastic, the discrete cracks are modeled using the nonlinear Interface Crack Model (ICM), while a nonlinear response of the passive steel is assumed by using J2 plasticity. The interface elements which model the discrete cracks are bridged by the 3D truss elements in order to model the continuity of the actual passive reinforcement and prestressing steel which would naturally span between any cracks in the containment ring.

The first of these analyses excludes the effect of pressurization of the open discrete cracks, while the second includes this effect. These analyses were run on a PC with a 1.7 GHz Pentium 4 processor and 256 MB of RAM. Both analyses were run to an internal pressure of 3 MPa in 75 load increments. The analysis without internal pressure ran with a CPU time of 9.5 minutes, while the analysis with internal pressure ran with a CPU time of 10.25 minutes. Convergence criteria was the following: (a) maximum number of iterations = 1000; energy error = 1.000; (c) relative residual error = 0.1000; (d) absolute residual error = 0.1000; and (e) displacement error = 0.0100.

Fig. 6 illustrates the deformed shape of the ring. We observe that the shape is controlled by the location of the ribs (which initially controlled the location of the cracks). Keeping in mind that the prestressing cables are located on the outside edge of the ring, we clearly have a mechanism at failure (here defined as maximum opening of all the cracks), where the ring is held together by the yielding steel, and the outside portion of the crack is closed as the two sides are in compression against each other.

A closer look at the ring, Fig. 7 highlights the kinematics of the ring under internal pressurization, crack opening from the inside, and closed crack on the outside.

Since the location of the discrete cracks and the deformation of the ring are symmetric, insight into the performance of the ring in relation to crack opening can be obtained by studying only one of the cracks. If gas leakage to the outside of the container is to be avoided, then one benchmark for “failure” of the ring is the point where the crack opening provides a clear path for gasses to travel from inside the ring to the outside. Crack opening versus internal pressure is plotted in Fig. 8 for both analysis cases, whereas the crack profile is shown in Fig. 9.

Finally Fig. 10 illustrates the deformed shape of the interface element by itself. The small overlap on the exterior of the ring is caused by the finite (yet large) stiffness given to the

interface element.

The first observation which can be made is that the cracks do not open until the internal pressure exceeds approximately 1.2 MPa. Below 1.2 MPa, the prestressing force in the ring is sufficient to hold the cracks closed. Above 1.2 MPa however, the confining effect of the prestressing is lost, and the internal pressure in the ring is high enough to open the cracks. This 1.2 MPa pressure threshold is consistent with the simple statics check in Appendix ??.

At pressures above 1.2 MPa, the cracks begin to open. Fig. 8 shows the crack opening at the crack mouth, which is at the interior face of the ring. However, gasses are only able to escape if there is a clear path through the ring from interior to exterior. The crack opening at the exterior face of the ring, is zero throughout the analysis. On the other hand, the crack opening inside the ring can be as high as 3 cm for an internal pressure of 3 MPa. It should be noted that at this internal pressure, the steel has yielded (thus causing the large opening), and concrete should have crushed (in this preliminary analysis we modeled the concrete as linear elastic material). Concrete compressive stresses were determined to range from 16 to 75 MPa for internal pressures of 1.6 and 3.0 MPa respectively. The concrete compressive strength is reached at an internal pressure of about 2.2 MPa. This highlights the need for a more refined analysis which accounts for concrete nonlinearity, as we would expect substantial leak to occur not only through the open crack, but also through the crushed concrete at a pressure of about 2.0 MPa. Hence, whereas local failure can be anticipated under high internal pressure, it is evident that we are in presence of a “leak-before-failure” scenario. That is at some point the internal pressure will be practically eliminated once there is a gas leakage.

Whereas one of the objectives of this present study was to determine the crack opening displacement profiles in order to assess gas flow, it is evident that internal pressurization of the crack does not greatly magnify the crack opening. This is due to the restraining effect of the prestressing steel.

Finally, a more rigorous analysis should also account for thermal load caused by the high temperature of the gas.

## 6 Conclusion

This paper has highlighted the applicability of a discrete crack model used in conjunction with a 3D nonlinear incremental analysis of a quasi-brittle material in presence of reinforcing and prestressing steel. Results, for the selected geometry indicate that:

- (1) A 3D mesh for this problem could relatively easily be put together with KumoNoSu.
- (2) The nonlinear analysis of a mesh with over twenty three thousand elements, eighteen thousand degrees of freedom, and seventy five increments, was accomplished in

around ten minutes on a personal computer.

- (3) Neglecting internal pressurization may be acceptable.
- (4) The mechanism associated with the eventual global failure of the ring was highlighted.
- (5) We have neglected to model thermal load, and the concrete material nonlinearity. Both could have been handled by MERLIN.

## 7 Acknowledgments

The financial support of the Tokyo Electric Power Service Company (TEPSCO), in the further development of Kumo and Merlin (originally developed under contract from the Electric Power Research Institute, EPRI) is gratefully acknowledged.



Fig. 6. Deformed Shape of the Ring

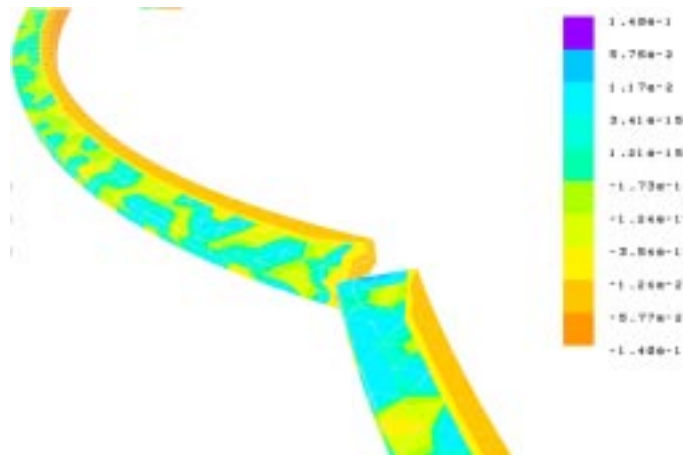


Fig. 7. Close-Up on the Deformed Shape of the Ring

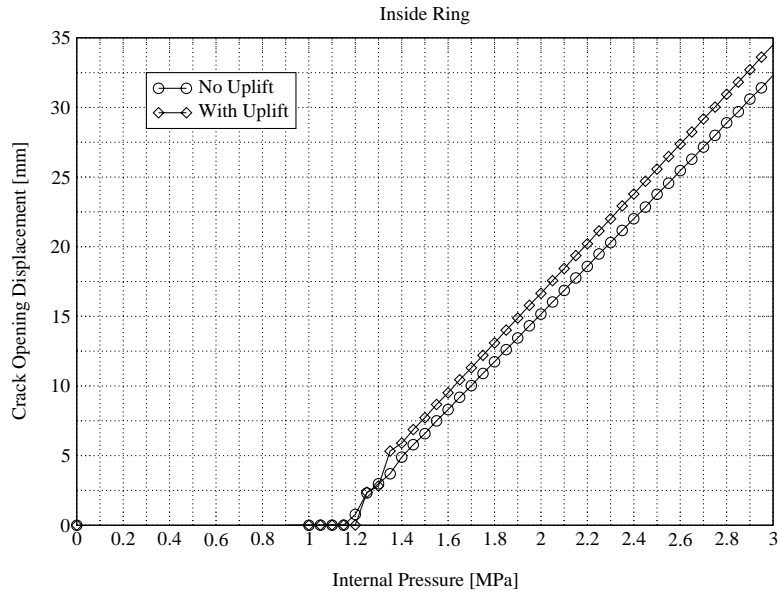


Fig. 8. Crack Opening Displacement in terms of Pressure

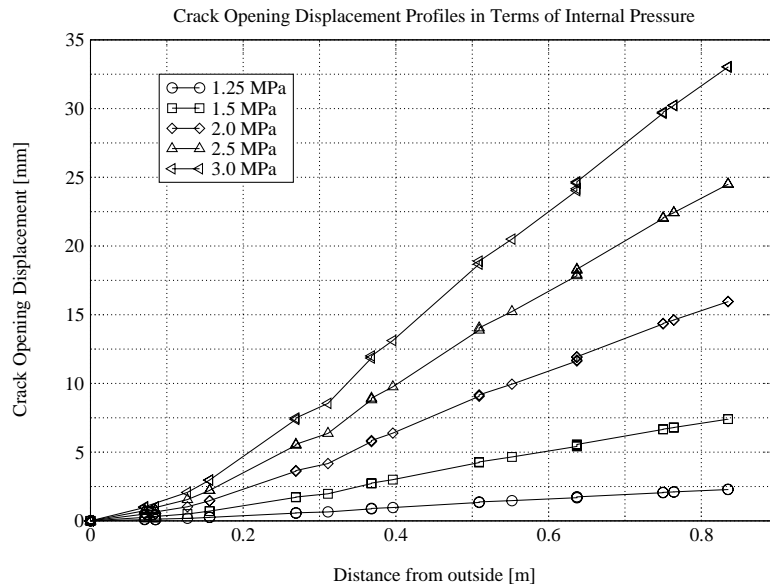


Fig. 9. Crack Opening Profiles

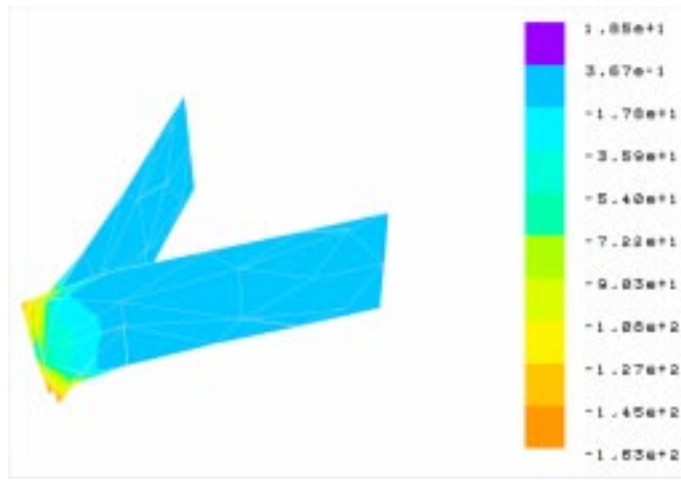


Fig. 10. Deformed Shape of Interface Element Along the Crack Surface

## References

- Bažant, Z.P. and Cedolin, L.: 1979, Blunt crack propagation in finite element analysis, *J. of the Engineering Mechanics Division, ASCE* **105**, 297–315.
- Belytschko, T. and Moës and Usui, S. and Parimi, C.: 2001, Arbitrary discontinuities in finite elements, *Int. J. Numer. Meth. Engng* **50**, 991–1013.
- Carol, I., Prat, P. and Lopez, C.: 1997, Normal/shear cracking model: Application to discrete crack analysis, *ASCE Journal of Engineering Mechanics*.
- Cervenka, J., Chandra Kishen, J. and Saouma, V.: 1998, Mixed mode fracture of cementitious bimaterial interfaces; part II: Numerical simulation, *Engineering Fracture Mechanics*.
- deBorst, R., Mazars, J., Pijaudier-Cabot, G. and vanMier, J. (eds): 2001, Balkema Publishers.
- Hansen, E. and Saouma, V.: 2001, KumoNoSu, a 3d interactive graphics mesh generator for merlin, *Technical report*, Report Submitted by the University of Colorado to the Tokyo Electric Power Service Company. <http://civil.colorado.edu/~saouma/Kumo>.
- Hansen, E. and Saouma, V.: 2002, Hibrid models for 3d reinforced concrete analysis, *Revue Francaise de Genie Civil*. In Print.
- Hansen, E., Willam, K. and Carol, I.: 2001, A two-surface anisotropic damage/plasticity model for plain concrete, in R. de Borst, J. Mazars, G. Pijaudier-Cabot and J. van Mier (eds), *Fracture Mechanics of Concrete Structures*, Balkema, Cachan.
- Hillerborg, A. and Modéer, M. and Petersson, P.E.: 1976, Analysis of crack formation and crack growth in concrete by means of fracture mechanics and finite elements, *Cement and Concrete Research* **6**(6), 773–782.
- Jirasek, M. and Bažant, Z.: 2001, *Inelastic Analysis of Structures*, John Wiley, Chichester.
- Mazars, J.: 1984, *Application de la Mécanique de L’Endommagement au Comportement Non Linéaire et a la Rupture du Béton de Structure*, PhD thesis, Ecole Normale Supérieure de l’Enseignement Technique, Université Pierre et Marie Curie, Cachan, France.
- Ngo, D. and Scordelis, A.: 1967, Finite element analysis of reinforced concrete beams, *Journal of the American Concrete Institute*.
- Nilson, A.: 1968, Nonlinear analysis of reinforced concrete by the finite element method, *Journal of the American Concrete Institute*.
- Oliver, J., Huespe, A., Pulido, M. and Chaves, E.: 2002, From continuum mechanics to fracture mechanics: The strong discontinuity approach, *Engineering Fracture Mechanics* **69**, 113–136.
- Rashid, Y.: 1968, Analysis of prestressed concrete pressure vessels, *Nuclear Engineering and Design*.
- Reich, R., Červenka, J. and Saouma, V.: 1997, Merlin, a three-dimensional finite element program based on a mixed-iterative solution strategy for problems in elasticity, plasticity, and linear and nonlinear fracture mechanics, *Technical report*, EPRI, Palo Alto. <http://civil.colorado.edu/~saouma/Merlin>.

Saouma, V.: 1980, *Finite Element Analysis of Reinforced Concrete; a Fracture Mechanics Approach*, PhD thesis, Cornell University, Department of Structural Engineering.

Sims, F., Rhodes, J. and Clough, R.: 1964, Cracking in norfolk dam, *J. of the American Concrete Institute*.